

The 3d O(4) model as an effective approach to the QCD phase diagram

E. López-Contreras, J. A. García-Hernández, E. N. Polanco-Euán, and W. Bietenholz

*Instituto de Ciencias Nucleares, Universidad Nacional Autónoma de México,
Apartado Postal 70-543, 04510 Ciudad de México, Mexico.*

Received 31 December 2021; accepted 2 May 2022

The QCD phase diagram is one of the most prominent outstanding puzzles within the Standard Model. Various experiments, which aim at its exploration beyond small baryon density, are operating or in preparation. From the theoretical side, this is an issue of non-perturbative QCD, and therefore of lattice simulations. However, a finite baryon density entails a technical problem (known as the “sign problem”), which has not been overcome so far. Here we present a study of an effective theory, the O(4) non-linear sigma model. It performs spontaneous symmetry breaking with the same Lie group structure as 2-flavor QCD in the chiral limit, which strongly suggests that they belong to the same universality class. Since we are interested in high temperature, we further assume dimensional reduction to the 3d O(4) model, which implies topological sectors. As pointed out by Skyrme, Wilczek and others, its topological charge takes the role of the baryon number. Hence the baryon chemical potential μ_B appears as an imaginary vacuum angle, which can be included in the lattice simulation without any sign problem. We present numerical results for the critical line in the chiral limit, and for the crossover in the presence of light quark masses. Their shapes are compatible with other predictions, but up to the value of about $\mu_B \approx 300$ MeV we do not find the notorious Critical Endpoint (CEP).

Keywords: QCD phase diagram; non-linear sigma model; lattice simulations.

DOI: <https://doi.org/10.31349/SuplRevMexFis.3.020727>

1. The QCD phase diagram

Beyond low baryon density, the QCD phase diagram is still *terra incognita*, both theoretically and experimentally (if we assume the validity of QCD as the correct theory of the strong interaction to persist). It can be parameterized by the inclusion of a baryonic chemical potential μ_B , which characterizes the density of the net baryon number $B - \bar{B}$, as sketched in Fig. 1.

It is often a good approximation to assume the light quark masses to be degenerate; we denote this mass as $m_q := m_u$

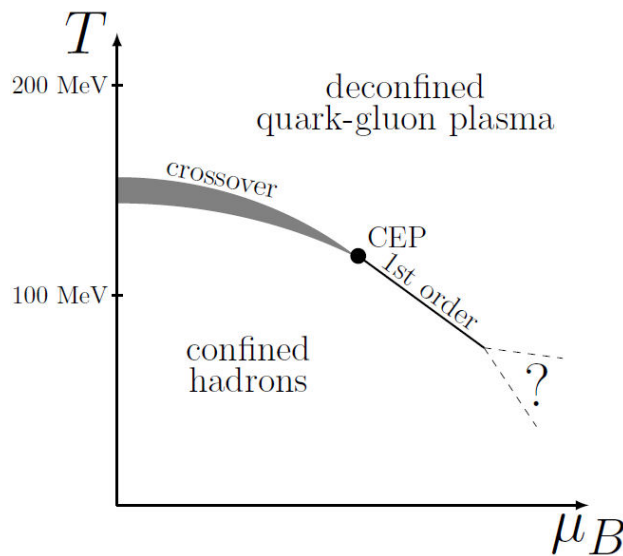


FIGURE 1. Symbolic illustration of the expected QCD phase diagram.

$= m_d$. In this setting, at $\mu_B = 0$, lattice QCD simulations provide the following results:

- In the chiral limit of u and d quarks, $m_q = 0$, one obtains a second order phase transition between the confined (hadronic) and deconfined phase (quark-gluon plasma). With the s -quark included, the critical temperature amounts to $T_c \simeq 132$ MeV [1]. If we still add the c -quark (with phenomenological values of m_s and m_c), the transition turns into a crossover, but its temperature hardly changes; one obtains the pseudo-critical temperature $T_{pc} \simeq 134$ MeV [2].
- For a realistic $m_q > 0$, and 2 or 2 + 1 flavors, one obtains a crossover as well. In the latter scenario, the pseudo-critical temperature is somewhat higher, $T_{pc} \simeq 155$ MeV [3]. This is consistent with the experimentally measured freeze-out temperature of the quark-gluon plasma.

This phase diagram is of interest *e.g.* for our understanding of the early Universe and of neutron stars. Several experiments are operating with the goal of exploring the nuclear phase diagram, at facilities like the Super Proton Synchrotron (SPS), the Relativistic Heavy Ion Collider (RHIC) and the Large Hadron Collider (LHC). Others are in preparation, we mention the Facility for Antiproton and Ion Research (FAIR), and in particular the Multi-Purpose Detector at the Nuclotron-based Ion Collider fAcility (MPD-NICA), which is under construction at JINR in Dubna, Russia [4], with the participation of the Mexican group MexNICA. It plans to collide heavy ions, such a bismuth nuclei, at energies of 4 to 11 GeV per nucleon, which is suitable to at-

tain a high baryon number density, and to access the region where one expects the Critical Endpoint (CEP), *i.e.* the point in the phase diagram where the crossover turns into a first order phase transition, cf. Fig. 1.

However, the location — and even the existence — of the CEP is uncertain. If it exists, one speculates about a rich phase structure at even higher μ_B , including for instance a color superconducting phase.

From the theoretical side, this is an issue of non-perturbative QCD, and therefore of lattice simulations, which did provide the aforementioned values of T_c and T_{pc} . It deals with the QCD formulation in Euclidean space-time, which is justified for equilibrium observables. One further assumes a discrete lattice structure, which implements an UV regularization. The quark fields ψ_x are formulated on the lattice sites x , and the gluon fields $U_{x,\mu}$ on the links connecting them (μ specifies the direction). It is profitable to use *compact* link variables in the gauge group (not in the algebra), $U_{x,\mu} \in \text{SU}(3)$, which avoids the need of gauge fixing. In analogy to Statistical Mechanics, one introduces the partition function in the functional integral formalism,

$$\begin{aligned} Z &= \int D\bar{\psi} D\psi DU e^{-S_{\text{quark}}[\bar{\psi}, \psi, U] - S_{\text{gauge}}[U]} \\ &= \int DU \det M[U] e^{-S_{\text{gauge}}[U]}. \end{aligned} \quad (1)$$

The factor $\det M[U]$ is the fermion determinant, which captures in particular the sea quark contributions. Its numerical computation is tedious, but one does not need to deal explicitly with the Grassmann-valued fields $\bar{\psi}$, ψ . Thus we obtain expectation values of observables, in particular n -point functions, as

$$\langle \dots \rangle = \frac{1}{Z} \int DU (\dots) \det M[U] e^{-S_{\text{gauge}}[U]}. \quad (2)$$

The method consists of generating a large set of gauge configurations $[U]$ with the probability distribution

$$p[U] = \frac{1}{Z} \det M[U] e^{-S_{\text{gauge}}[U]}, \quad (3)$$

which enables the numerical measurement of $\langle \dots \rangle$. Here we assume the Euclidean action $S_{\text{QCD}} = -\ln \det M[U] + S_{\text{gauge}}[U]$ to be real positive, and we see that the Euclidean space is vital.

This method provides results with statistical errors (due to the finite set of configurations), and systematic errors (we need to extrapolate to the continuum and to infinite volume), but they are controlled and additional simulations reduce them. This approach is fully *non-perturbative*: a strong coupling like $\alpha_s = \mathcal{O}(1)$ does not cause any problem.

The temperature T is given by the inverse extent in Euclidean time, which should be much shorter than the spatial directions to obtain results at finite T . This is how T_c and T_{pc} were obtained.

However, adding a chemical potential $\mu_B > 0$ leads to a serious difficulty known as the “sign problem”. We can interpret μ_B as the energy, which is required for adding one more baryon. It multiplies a real Lagrangian term in Minkowski space, but this term becomes imaginary under Wick rotation. With this term, $\det M$, and therefore also the Euclidean action S_{QCD} , is complex, so $(1/Z) \exp(-S_{\text{QCD}})$ does not represent a probability anymore. In this case (and similarly in the presence of a θ -term), the standard technique that we sketched above does not apply.

Numerous attempts have been studied to overcome the sign problem, but there is no breakthrough so far. For comprehensive reviews, we refer for instance to Refs. [5].

- The straight approach is simulating with probability $p \propto \exp(-\text{Re } S_{\text{QCD}})$, and including the complex phase *a posteriori* by re-weighting. This is correct in principle, but it leads to excessive cancellations, such that a precise result requires huge statistics. With stable statistical errors, the requested statistics grows exponentially with the volume, which often makes this approach hopeless.
- The complex Langevin algorithm can handle and update a complex action, but the link variables leave the gauge group $\text{SU}(3)$.
- Some collaborations simulate at imaginary chemical potential, $\mu_B^2 < 0$, and try to extrapolate to $\mu_B^2 > 0$.
- At $\mu_B = 0$ it is possible to compute some coefficients of the Taylor series of the crossover curve, which extends to $\mu_B > 0$.

Unfortunately none of these approaches is really conclusive regarding the search for the CEP.

Quantum computing offers some hope: it would allow us to directly deal with $S_{\text{QCD}} \in \mathbb{C}$. This is under intense investigation in toy models, but not yet applicable to QCD. We mention one example, which refers to analogue quantum computing, with Mexican participation [6]: if one traps suitable, ultra-cold alkaline-earth atoms in the nodes of a 2d optical lattice, the nuclear spins represent an $\text{SU}(3)$ field, which may perform Spontaneous Symmetry Breaking (SSB), $\text{SU}(3) \rightarrow \text{U}(2)$. Then the low-energy effective action of the Nambu-Goldstone bosons just corresponds to the 2d $\mathbb{CP}(2)$ model, which could be quantum simulated in this manner, and which bears a number of similarities with QCD (asymptotic freedom, topology, a dynamically generated mass gap).

In the absence of conclusive QCD results, one derives conjectures about the QCD phase diagram from related models. Many such models have been studied. Examples, and corresponding references, include the Nambu-Jona-Lasinio model [7], and more specifically the Polyakov-Nambu-Jona-Lasinio model [8], the linear σ -model [9], holographic approaches to QCD [10], the Polyakov quark meson model [11], as well as methods like the Dyson-Schwinger equation [12], the mean-field approximation [13] and finite-size scaling [14].

As a new approach, here we focus on the 3d O(4) non-linear σ -model, with an imaginary θ -term.

2. The 3d O(4) model as an effective theory

2.1. 2-flavor QCD

Two quark flavors are very light compared to the intrinsic scale of QCD, $m_u \simeq m_d \ll \Lambda_{\text{QCD}} \approx 300$ MeV, hence the chiral limit $m_q := m_u = m_d = 0$ is often a good approximation. (For instance, the nucleon mass is only modified by a few percent, which shows that the mass of macroscopic objects is mostly due to the gluon energy, and only to a minor part due to the Higgs mechanism.) In this limit, the left- and right-handed quarks decouple,

$$\mathcal{L}_{\text{quark}} = (\bar{u}, \bar{d})_L \gamma_\mu D_\mu \begin{pmatrix} u \\ d \end{pmatrix}_L + (\bar{u}, \bar{d})_R \gamma_\mu D_\mu \begin{pmatrix} u \\ d \end{pmatrix}_R,$$

so the corresponding quark doublets can be transformed independently, and the QCD Lagrangian has the global symmetry

$$\begin{aligned} \text{U}(2)_L \otimes \text{U}(2)_R &= \text{SU}(2)_L \otimes \text{SU}(2)_R \\ &\otimes \text{U}(1)_{L=R} \otimes \text{U}(1)_{\text{axial}}. \end{aligned}$$

The $\text{U}(1)_{L=R}$ symmetry assures the fermion number conservation, while the axial symmetry $\text{U}(1)_{\text{axial}}$ is anomalous (explicitly broken under quantization). At $T < T_c$ the remaining chiral flavor symmetry undergoes SSB,

$$\text{SU}(2)_L \otimes \text{SU}(2)_R \longrightarrow \text{SU}(2)_{L=R}, \quad (4)$$

which — according to Goldstone’s Theorem — generates 3 Nambu-Goldstone bosons. If we add small quark masses to the u - and d -quark, they become massive, because the symmetry breaking has a (small) explicit component, and these quasi-Nambu-Goldstone are identified with the pions.

2.2. The O(4) model as an effective theory

We proceed to the O(4) non-linear σ -model as an effective theory with an equivalent SSB pattern. Its action reads

$$S[\vec{e}] = \int d^4x \left[\frac{F_\pi^2}{2} \partial_\mu \vec{e}(x) \cdot \partial_\mu \vec{e}(x) - \vec{h} \cdot \vec{e}(x) \right], \quad (5)$$

with $\vec{e}(x) \in S^3$, and \vec{h} is an external “magnetic field” (or “ordering field”). According to Chiral Perturbation Theory, $F_\pi \simeq 92.4$ MeV is the pion decay constant.

At $\vec{h} = \vec{0}$ the action has a global O(4) symmetry, which can break spontaneously to O(3) (“spontaneous magnetization”). $\vec{h} \neq \vec{0}$ adds some explicit symmetry breaking, like the

(degenerate) quark mass $m_q > 0$. The symmetry groups with or without SSB, or quasi-SSB, are locally isomorphic,

$$\{ \text{SU}(2)_L \otimes \text{SU}(2)_R \hat{=} \text{O}(4) \} \longrightarrow \{ \text{SU}(2)_{L=R} \hat{=} \text{O}(3) \}.$$

The SSB pattern and the space-time dimension usually determine the universality class at criticality, so we have a strong reason to assume the O(4) model to belong to the same universality class as 2-flavor QCD, cf. Refs. [15].

In the broken phase, it can be regarded as an effective pion model, as in Chiral Perturbation Theory, since the field is defined in the SSB coset space, $\vec{e} \in S^3 = \text{O}(4)/\text{O}(3)$. Hence we deal with a meson field, so how can we address the baryon number?

Unlike Chiral Perturbation Theory, we are interested in high $T = 1/\beta$. We assume it to be high enough for dimensional reduction to be a good approximation, *i.e.* we assume the dominant configurations $[\vec{e}]$ to be (nearly) constant in the (short and periodic) Euclidean time direction.ⁱ This reduces the temporal integral in the action (5) to a constant, $\int_0^\beta dt_E \approx \beta$, and we obtain (in a spatial volume V)

$$\begin{aligned} S[\vec{e}] &= \beta \int_V d^3x \left[\frac{F_\pi^2}{2} \partial_i \vec{e}(x) \cdot \partial_i \vec{e}(x) - \vec{h} \cdot \vec{e}(x) \right] \\ &= \beta H[\vec{e}]. \end{aligned} \quad (6)$$

Thus we arrive at the 3d O(4) model, with periodic boundary conditions, which has topological sectors, due to $\pi_3(S^3) = \mathbb{Z}$. The topological charge $Q \in \mathbb{Z}$ represents the winding number of a configuration $[\vec{e}]$ on S^3 , which is invariant under (almost all) small deformations of $[\vec{e}]$.

Skyrme and others noticed that the topological charge Q of the effective theory corresponds to the baryon number B [17]. This identification can be derived from anomaly matching. Thus the meson field does account for the baryon number, by means of topological windings. Hence in the effective theory, the baryonic chemical potential μ_B takes the role of an imaginary vacuum-angle θ ,

$$H[\vec{e}] = \dots - \mu_B Q[\vec{e}] \in \mathbb{R}. \quad (7)$$

We see that it can be incorporated in the effective theory *without* any sign problem.

2.3. The 3d O(4) model on the lattice

In order to simulate the 3d O(4) model we need to formulate it on the lattice. We choose the standard formulation on a cubic lattice, and use lattice units (*i.e.* we set the lattice spacing to 1). The derivatives are replaced by nearest-neighbor differences,

ⁱ This assumption can be questioned, *i.e.* one may wonder whether $1/T_{\text{pc}} \simeq 1.3$ fm is small enough to justify this simplification. One can further object that at high- T heavier quark flavors are not negligible, but we cannot include them in O(N) model effective theories [16]. Still, we are confident that our assumptions are sensible approximations.

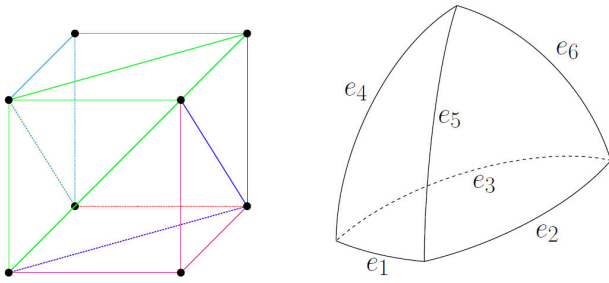


FIGURE 2. Left: Division of a lattice unit cube into 6 tetrahedra. Right: Symbolic illustration of a spherical tetrahedron.

$$\frac{1}{2} \partial_i \vec{e}(x) \cdot \partial_i \vec{e}(x) \rightarrow \frac{1}{2} (\vec{e}_{x+\hat{i}} - \vec{e}_x)^2 = 1 - \vec{e}_x \cdot \vec{e}_{x+\hat{i}},$$

$$S_{\text{lat}}[\vec{e}] = -\beta_{\text{lat}} \left(\sum_{\langle xy \rangle} \vec{e}_x \cdot \vec{e}_y + \vec{h}_{\text{lat}} \cdot \sum_x \vec{e}_x \right) + \mu_{B,\text{lat}} Q[\vec{e}],$$

where \hat{i} is a unit vector in i -direction, and $\langle xy \rangle$ are the nearest-neighbor lattice sites (the constant 1 can be dropped).

We formulate the topological charge of a lattice configuration with a geometric definition. Thus we generalize the formulation of Ref. [18], which guarantees $Q[\vec{e}] \in \mathbb{Z}$ for all configurations (up to a subset of measure zero).

To be explicit, we split the lattice unit cubes into 6 tetrahedra, as shown in Fig. 2 (left). The 4 spins at the vertices of one tetrahedron — we call them $(\vec{e}_w, \vec{e}_x, \vec{e}_y, \vec{e}_z)$ — span a *spherical tetrahedron* on S^3 , as symbolically sketched in Fig. 2 (right): its edges e_1, \dots, e_6 are geodesics in S^3 .

The topological density of a tetrahedron is given by the oriented, normalized volume of its corresponding spherical tetrahedron, $V_{w,x,y,z}[\vec{e}]/2\pi^2$, such that

$$Q[\vec{e}] = \frac{1}{2\pi^2} \sum_{\langle wxyz \rangle} V_{w,x,y,z}[\vec{e}] \in \mathbb{Z}. \quad (8)$$

Remarkably, it was only in 2012 that a set of formulae was elaborated which allow for the computation of $V_{w,x,y,z}[\vec{e}]$ [19]. It can be numerically computed in this manner [20], but a more efficient alternative is selecting some reference point on S^3 and counting how many spherical tetrahedra enclose it in an oriented sense (we tested extensively the equivalence of these two methods).

2.4. Monte Carlo simulation

As we anticipated in Sec. 1, the goal is the generation of numerous configurations in accordance with the probability distribution $p[\vec{e}] = (1/Z) \exp(-S[\vec{e}])$.

We start from an arbitrary initial configuration $[\vec{e}]$ and generate a long Markov chain $[\vec{e}] \rightarrow [\vec{e}'] \rightarrow [\vec{e}'] \rightarrow \dots$ (each new configuration solely depends on the previous one,

plus some random numbers). The conditions for the algorithm to be correct are *ergodicity* (each configuration is accessible in a finite number of steps) and *detailed balance*: the transition probabilities between two configurations obey

$$\frac{p[\vec{e} \rightarrow \vec{e}']}{p[\vec{e}' \rightarrow \vec{e}]} = \frac{p[\vec{e}']}{p[\vec{e}]} = \exp(S[\vec{e}] - S[\vec{e}']). \quad (9)$$

One begins with the *thermalization*: first a large number of configurations are skipped, until we reach thermal equilibrium (and therefore independence of the initial configuration). Then we perform numerical measurements on configurations, which have to be sufficiently separated in the Markov chain to be statistically independent from each other. To assure this property, we measure the (exponential) auto-correlation “time” τ ; it is very similar for the different observables involved (see below). We are on the safe side with a measurement separation $\geq 2\tau$.

τ grows rapidly next to the critical temperature. For typical algorithms it diverges at T_c in infinite volume, and the increase when T approaches T_c is exponential: this phenomenon is known as *critical slowing down*.

By definition, also the correlation length diverges at a critical point, $\xi \rightarrow \infty$. Thus the spins are strongly correlated over long distances (in lattice units), which explains that it becomes hard to significantly modify a configuration (while respecting detailed balance).

For the $O(N)$ models, the Wolff cluster algorithm [21] is the most efficient, known simulation procedure. It does not update single spins, but entire clusters of them are reflected at some random hyper-plane in spin-space (they are “flipped”). The clusters are formed in a subtle manner, such that the algorithm fulfills the aforementioned conditions of ergodicity and detailed balance.

We used the multi-cluster version (but we also checked its consistency with the single-cluster algorithm). One multi-cluster update step means that the entire configuration is divided into clusters, which are flipped with the appropriate probability. The availability of this highly efficient algorithm is another benefit of the $O(4)$ model as an effective theory; no efficient cluster algorithm is known in gauge theory. We take the chemical potential μ_B into account by adjusting the cluster flip probability, along the lines of Ref. [22]. This method works consistently, but when $\mu_{B,\text{lat}}$ increases, the peak height of τ grows rapidly.

This is illustrated in Fig. 3 for the auto-correlation “times” with respect to the energy, τ_H , and the topological charge, τ_Q . They are very similar, thanks to the cluster algorithm (for single-spin update algorithms, τ_Q tends to be much larger and to restrict the feasibility of conclusive simulations).

We see that not even the cluster algorithm completely overcomes the problem of critical slowing down. This difficulty has limited our numerical study so far to $\mu_{B,\text{lat}} \leq 2.5$. On the other hand, the sharp peaks of τ provide a first estimate of the critical value $\beta_{c,\text{lat}}$.

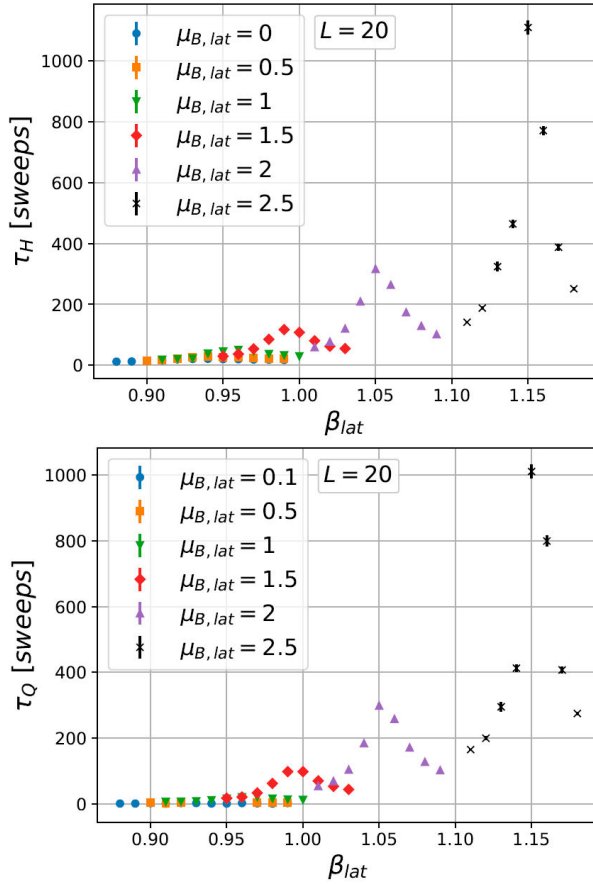


FIGURE 3. The auto-correlation “time” with respect to the energy, τ_H (top) and with respect to the topological charge, τ_Q (bottom), expressed in units of multi-cluster update steps (“sweeps”). These values are measured in the chiral limit ($\vec{h}_{\text{lat}} = \vec{0}$) by the exponential decay of the auto-correlation.

3. Results for the phase diagram in the chiral limit

We begin with the case $\vec{h}_{\text{lat}} = \vec{0}$, which corresponds to zero quark and pion masses. Before showing our simulation results, which are based on Ref. [23], we address the conversion from lattice units to physical units. This requires some reference quantity as an input. Here, we refer to the critical temperature $T_c = 1/\beta_c$ at $\mu_B = 0$. In the 3d O(4) model on the lattice, it was measured to high precision [24–26]; we are going to refer to $\beta_{c,\text{lat}} = 0.9359(1)$. We match this result to $T_c \simeq 132$ MeV, the value obtained in chiral lattice QCD [1] (cf. Sec. 1), which suggests

$$\mu_B = \frac{\beta_{c,\text{lat}}}{\beta_c} \mu_{B,\text{lat}} \approx 124 \text{ MeV } \mu_{B,\text{lat}}. \quad (10)$$

Our simulation parameters are

$$\mu_{B,\text{lat}} = 0, 0.1, 0.2 \dots 1.5; 2, 2.5 \Leftrightarrow \mu_B = 0 \dots 309 \text{ MeV}.$$

The lattice volumes are cubic, $V = L^3$, $L = 10, 12, 16, 20$, and, if not indicated otherwise, we will show results for

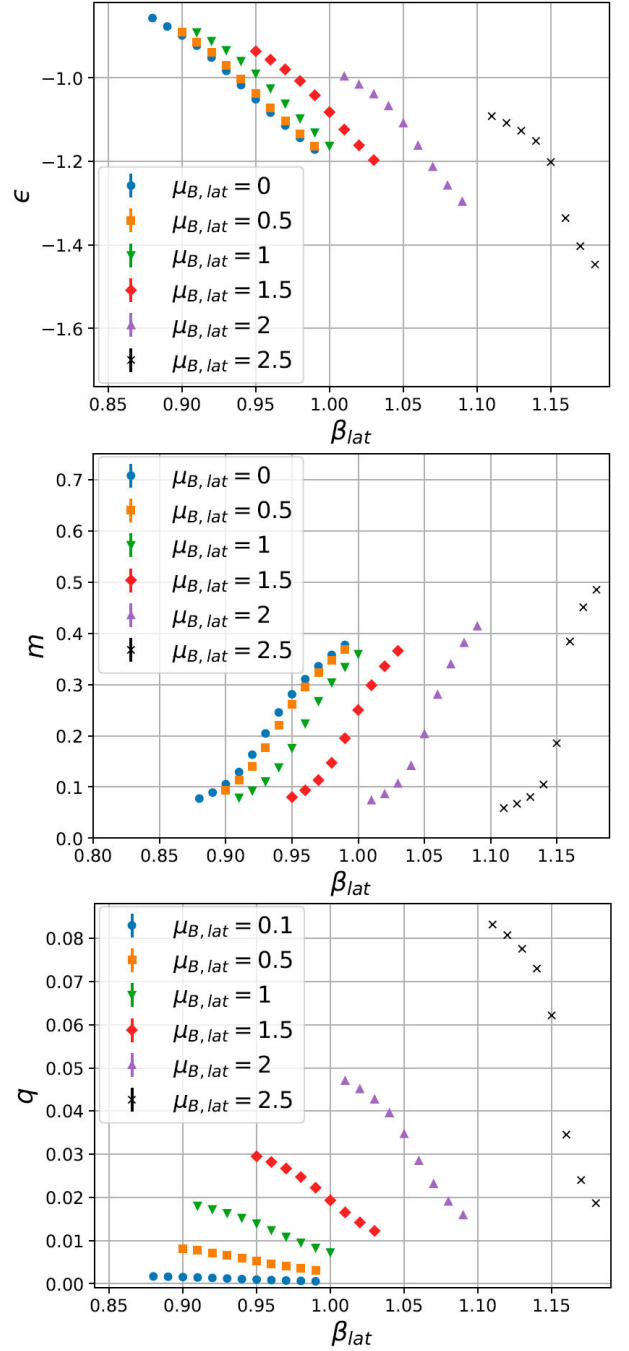


FIGURE 4. Energy density ϵ , magnetization density m and topological density q , at $L = 20$, $\vec{h} = \vec{0}$ and $\mu_{B,\text{lat}} = 0 \dots 2.5$.

$L = 20$. The β_{lat} -values are chosen such that $\beta_{c,\text{lat}}$ can be identified — this had to be explored at each $\mu_{B,\text{lat}}$.

We measured observables which are given by first and second derivatives of the free energy $F = -T \ln Z$. According to Ehrenfest’s scheme, a discontinuity in the n^{th} derivative (in the large- L limit) characterizes an n^{th} order phase transition. We monitor the critical line and search in particular for a possible CEP, as motivated in Sec. 1. Each measurement is based on 10^4 (thermalized and decorrelated) configurations.

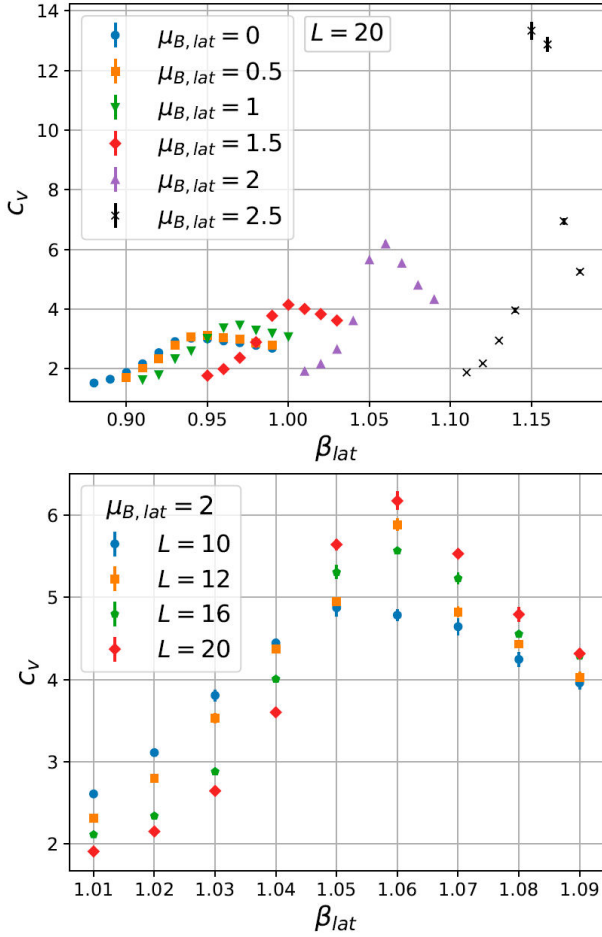


FIGURE 5. The specific heat c_V at $L = 20$ (top) and at $\mu_{B,\text{lat}} = 2$ (bottom). The peaks hint at second order phase transitions in the large- L limit. The L -dependence of their heights provides information about the critical exponents α and ν .

Figure 4 shows the energy density ϵ , the magnetization density m (the order parameter) and the topological density q , which are all given by first derivatives of F ,ⁱⁱ

$$\begin{aligned} \epsilon &= \langle H \rangle / V = \frac{1}{V} \partial_\beta (\beta F), \\ m &= \langle |\vec{M}| \rangle / V, \quad \langle \vec{M} \rangle = \left\langle \sum_x \vec{e}_x \right\rangle = -\partial_{\vec{h}} F, \\ q &= \langle Q \rangle / V, \quad \langle Q \rangle = -\partial_{\mu_B} F. \end{aligned} \quad (11)$$

Increasing $\mu_{B,\text{lat}}$ favors more topological windings. This enhances q and also ϵ , but it reduces m , since the configurations are further away from a uniform structure. Clearly, increasing β_{lat} has the opposite effect. In all three plots we see intervals of maximal slope, which move to large β_{lat} when $\mu_{B,\text{lat}}$ grows: this indicates the approximate value of $\beta_{c,\text{lat}}$,

in agreement with the peaks of the auto-correlation “times” in Fig. 3.

For $\mu_{B,\text{lat}} = 2.5$ these slopes are so strong that one could even be tempted to interpret them as quasi-discontinuous jumps, *i.e.* they could indicate discontinuous jumps in the large- L limit. That would be characteristic of a *first* order phase transition, so at this point we wonder whether the CEP has been attained already. This has to be clarified by the study of further observables, which are given by second derivatives of the free energy F .

In this respect, we first consider the specific heat c_V ,

$$c_V = \frac{\beta^2}{V} (\langle H^2 \rangle - \langle H \rangle^2) = -\frac{\beta^2}{V} \partial_\beta^2 (\beta F). \quad (12)$$

In infinite volume it diverges at a second order phase transition. In Fig. 5 (top) we see peaks with increasing height when $\mu_{B,\text{lat}}$ rises. This indicates that the phase transition at these parameters, in infinite volume, is still second order.

This is more explicit in Fig. 5 (bottom), which compares $c_V(\beta_{\text{lat}})$ in different volumes. The peak centers hardly depend on L , which makes their large- L extrapolation simple. Based on finite-size scaling one expects (assuming $L = \infty$ to be a critical point) a peak height proportional to $L^{\alpha/\nu}$. At $\mu_{B,\text{lat}} = 2$ we obtain for the ratio of these critical exponents $\alpha/\nu \approx 0.2$. If we further assume Josephson’s scaling law $\alpha = 2 - d\nu$, we arrive at $\alpha \approx 1/8$, $\nu \approx 5/8$. As a benchmark, Ref. [24] obtained at $\mu_{B,\text{lat}} = 0$ the value $\nu \simeq 0.7479(90)$, which is in reasonable proximity.

Similarly, in Fig. 6 (top) we show results for the magnetic susceptibility χ_m at $L = 20$,

$$\chi_m = \frac{\beta}{V} (\langle \vec{M}^2 \rangle - \langle |\vec{M}| \rangle^2) \sim -\frac{\beta}{V} \partial_{\vec{h}}^2 F. \quad (13)$$

(In a numerical study, the subtracted term is only sensible with $|\vec{M}|$, see *e.g.* Ref. [27]. The right-hand side, however, is the standard formula, without absolute value). It also diverges at T_c in infinite volume, hence its peaks in finite volume are another indicator of a second order phase transition. They are strongest at $\mu_{B,\text{lat}} \geq 1$, which supports the scenario that we are still following a critical line.

The plot in Fig. 6 (bottom) shows results for $L = 10 \dots 20$ at $\mu_{B,\text{lat}} = 2.5$. Here, the peak temperature visually moves with L , and the large- L extrapolation is compatible with the estimates for T_c based on the previous criteria. In this case, one expects (peak height) $\propto L^{\gamma/\nu}$. In the range $\mu_{B,\text{lat}} \leq 1.5$ this yields $\gamma/\nu = 1.9(2)$ [23], in agreement with the precise value $\gamma/\nu = 1.970$ at $\mu_{B,\text{lat}} = 0$ [26].

Figure 7 adds results about the topological susceptibility

$$\chi_t = \frac{1}{V} (\langle Q^2 \rangle - \langle Q \rangle^2) = -\frac{1}{V} \partial_{\mu_B}^2 F. \quad (14)$$

ⁱⁱ In Eqs. (11), (12) and (13), β and μ_B are understood as β_{lat} and $\mu_{B,\text{lat}}$ for the interpretation of our data.

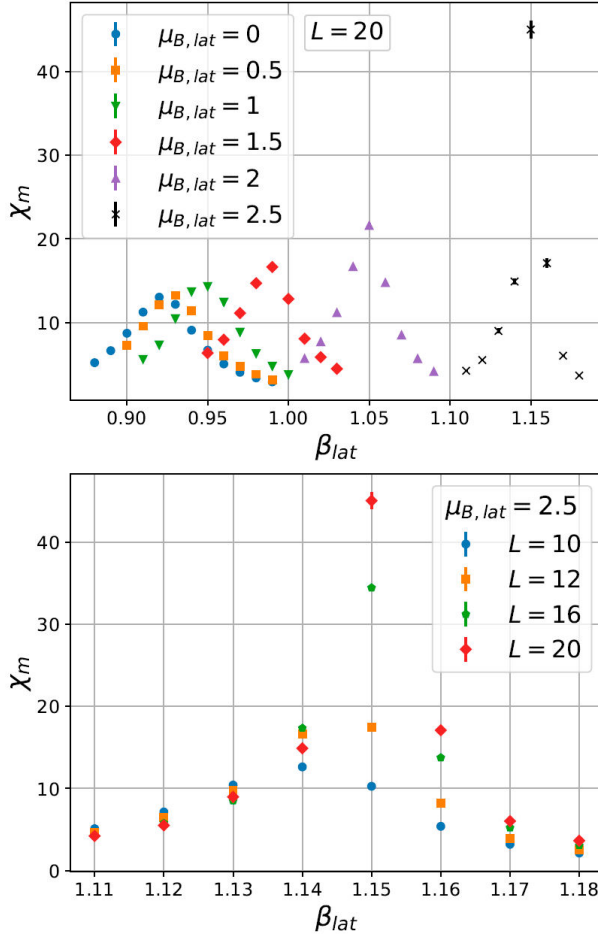


FIGURE 6. The magnetic susceptibility χ_m at $L = 20$ (top) and at $\mu_{B,lat} = 2$ (bottom). The peaks again hint at second order phase transitions in the large- L limit. The L -dependence of their heights provides information about the ratio of critical exponents γ/ν .

Again we observe peaks (they are obvious at $\mu_{B,lat} \geq 2$), at temperatures which are consistent with the previous determinations of T_c . Regarding the peak height, in analogy to Figs. 5 and 6, one might define a critical exponent ζ by the relation $\chi_t(T_c) \propto L^{\zeta/\nu}$, for which we obtain *e.g.*

$$\frac{\zeta}{\nu} \approx \begin{cases} 0.2 & \mu_{B,lat}=0 \\ 0.3 & \mu_{B,lat}=1 \end{cases}. \quad (15)$$

Taking all these results for quantities given by second derivatives of F together, strongly supports the scenario of a second order phase transition, all the way up to $\mu_{B,lat} = 2.5$. If we combine all the indications for the values of $\beta_{c,lat}(\mu_{B,lat})$ (peaks and steepest slopes), extrapolate to the thermodynamic limit $L \rightarrow \infty$, and convert the outcome into physical units, we arrive at our conjecture for the chiral phase diagram in Fig. 8. We see that T_c decreases monotonically with increasing baryon density, as generally expected. According to this diagram, a possible CEP should be located at $\mu_B > 309$ MeV and $T < 106$ MeV.

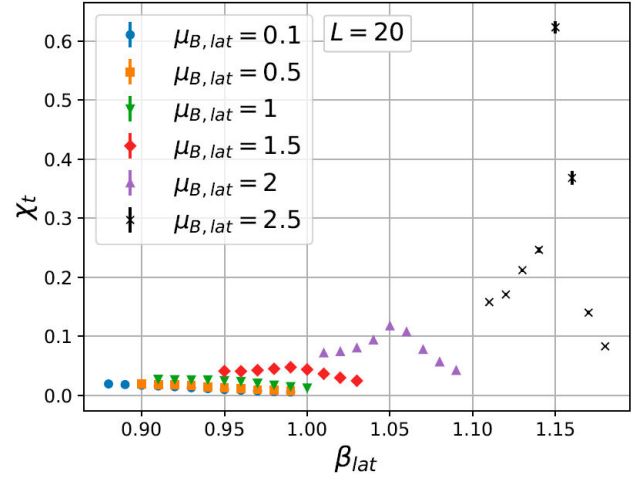


FIGURE 7. The topological susceptibility χ_t at $L = 20$. The peaks at $\mu_{B,lat} = 2$ and 2.5 further support the scenario of a second order phase transition.

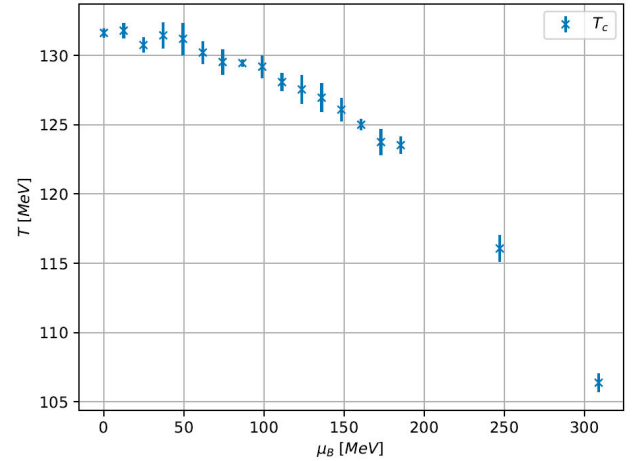


FIGURE 8. Conjectured phase diagram of 2-flavor QCD in the chiral limit.

4. Results with light quarks

We repeat that the O(4) model represents an effective theory for 2-flavor QCD, where a “magnetic field” $h = |\vec{h}|$ plays a role analogous to a degenerate quark mass $m_q = m_u = m_d$. This is the parameter which adds some explicit symmetry breaking, and gives mass to the pions (this is well-known in Chiral Perturbation Theory).

We simulated at two values of this parameter, in lattice units they amount to $h_{lat} = 0.14$ and $h_{lat} = 0.367$. For the conversion between lattice units and physical units, we now refer to the phenomenological, pseudo-critical crossover temperature $T_{pc} \simeq 155$ MeV at zero baryon density [3]. Our simulation results for $T_{pc,lat}$ are ambiguous, as expected for a crossover, see below. We anticipate the mean values in lattice units at $\mu_{B,lat} = 0$ (at this point without uncertainties),

$$\bar{T}_{\text{pc,lat}} = \begin{cases} 1.172 & h_{\text{lat}} = 0.14 \\ 1.273 & h_{\text{lat}} = 0.367 \end{cases}$$

$$\Rightarrow \mu_B = \frac{T_{\text{pc}}}{\bar{T}_{\text{pc,lat}}} \mu_{B,\text{lat}}$$

$$= \begin{cases} 132 \text{ MeV } \mu_{B,\text{lat}} & h_{\text{lat}} = 0.14 \\ 122 \text{ MeV } \mu_{B,\text{lat}} & h_{\text{lat}} = 0.367 \end{cases} \quad (16)$$

Still following the analogy to QCD, we interpret the chiral symmetry breaking parameter as

$$h = \frac{T_{\text{pc}}^4}{\bar{T}_{\text{pc,lat}}^4} h_{\text{lat}} = m_q \Sigma, \quad (17)$$

with the chiral condensate $\Sigma = -\langle \bar{\psi}\psi \rangle \approx (250 \text{ MeV})^3$, which allows us to estimate the physical values of the quark mass,

$$m_q \approx \begin{cases} 3 \text{ MeV} & h_{\text{lat}} = 0.14 \\ 5 \text{ MeV} & h_{\text{lat}} = 0.367 \end{cases} \quad (18)$$

We include also this symmetry-breaking term in the cluster algorithm by modifying the cluster-flip probability, as described in Refs. [28,29]. The magnitude of the auto-correlation time τ is strongly alleviated compared to Sec. 3, see Fig. 9, since the critical line is replaced by a crossover. τ does not diverge at β_{pc} in infinite volume, hence there is no critical slowing down in this case. Thus the massive model is computationally less demanding, which allowed us to include $L = 24$, and larger volumes are accessible as well; this is work in progress.

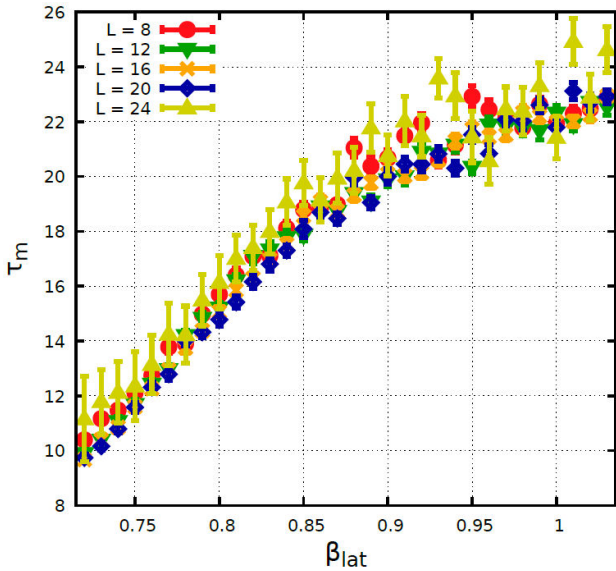


FIGURE 9. Auto-correlation “time” with respect to the magnetization in units of multi-cluster update steps. There is only a minor dependence on the size L , and no critical slowing down.

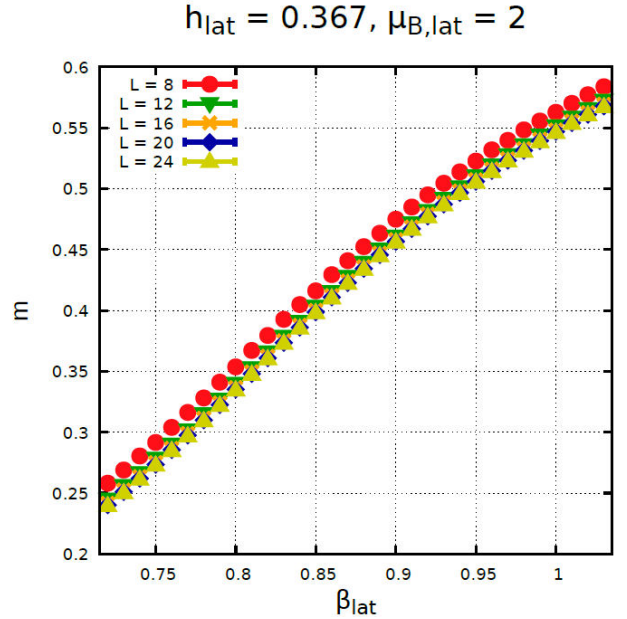
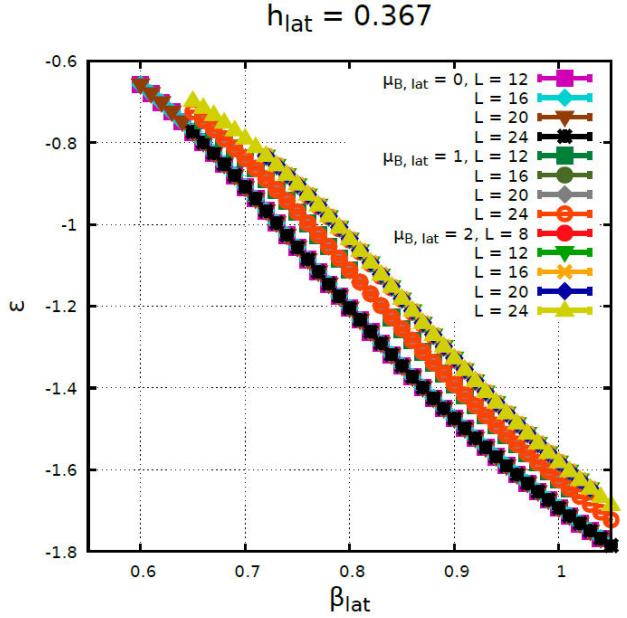


FIGURE 10. Energy density ϵ and magnetic density m at $h_{\text{lat}} = 0.367$. We see shifts depending on $\mu_{B,\text{lat}}$, but no interval of extraordinary slopes, since the second order phase transition (at $h_{\text{lat}} = 0$) is now washed out to a crossover. Modest finite-size effects are visible for m .

So far our simulation parameters are

$$V = L^3, \quad L = 8, 12, 16, 20, 24;$$

$$\mu_{B,\text{lat}} = 0 \dots 2. \quad (19)$$

At $h_{\text{lat}} = 0.14$ we have additional data at $\mu_{B,\text{lat}} = 2.5$, which corresponds to $\approx 330 \text{ MeV}$.

In the following, we are going to show results for $h_{\text{lat}} = 0.367$ at β_{lat} -values in the crossover region, again based on 10^4 measurements at each parameter set, for similar observables as in Sec. 3, following Ref. [29]. The results at

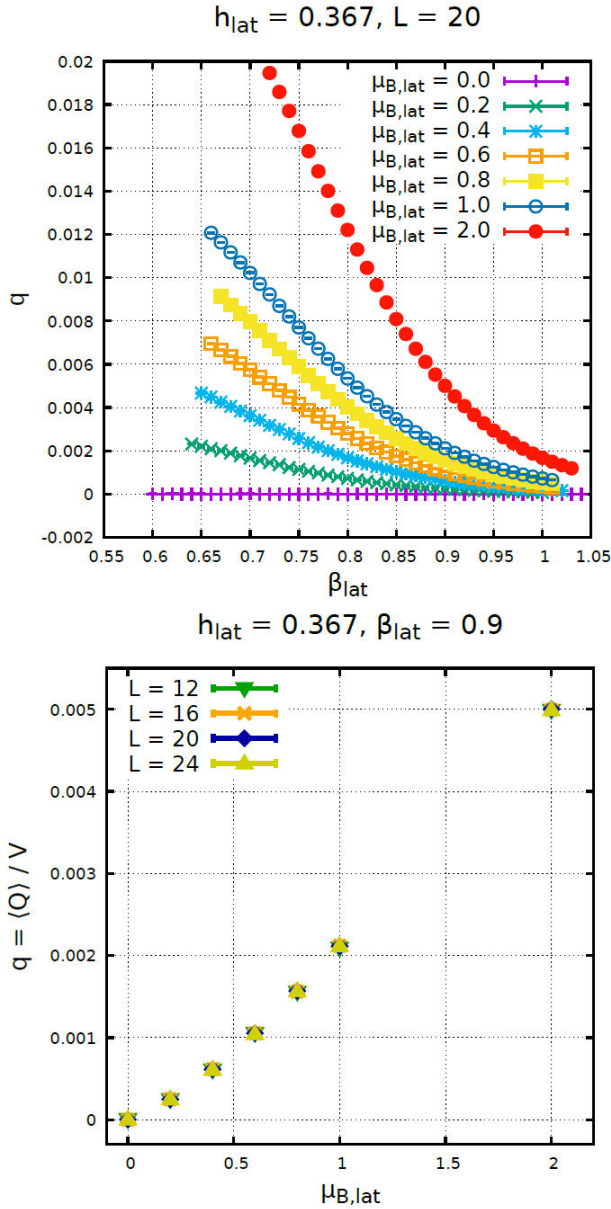


FIGURE 11. The topological density $q = \langle Q \rangle / V$ as function of β_{lat} at $L = 20$ (top), and at $\beta_{\text{lat}} = 0.9$ in different volumes (bottom). We see how an increasing $\mu_{B,\text{lat}}$ enhances q , whereas increasing β_{lat} suppresses it. At $L \geq 12$ there are hardly any finite-size effects on q .

$h_{\text{lat}} = 0.14$ look alike; they will be included in our final conjecture about the phase diagram in the massive case.

Figure 9 shows the auto-correlation “time” with respect to the magnetization, τ_m : the absence of critical slowing down is obvious, so we are on the safe side if we separate the measurements by 45 multi-cluster update steps. On the other hand, in contrast to the chiral case, τ_m does not provide a first estimate for $\beta_{\text{pc,lat}}$.

In Fig. 10 we proceed to the energy density ϵ and the magnetization density m , cf. Eqs. (11). Only for m modest finite-size effects are visible, but changing $\mu_{B,\text{lat}}$ causes a shift in ϵ . In either case, there is no interval of an extraordi-

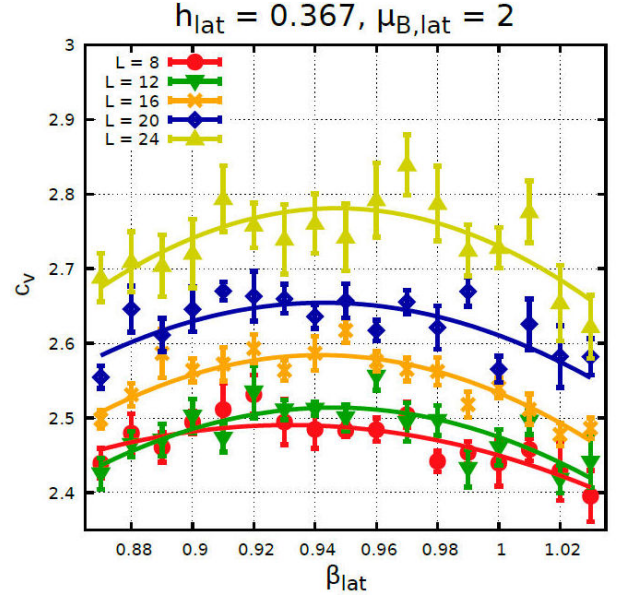


FIGURE 12. The specific heat c_V at $\mu_{B,\text{lat}} = 2$ as a function of β_{lat} , in various volumes. The peaks are smeared out due to $h_{\text{lat}} > 0$. We localize the maxima $\beta_{\text{max,lat}}$ by Gaussian fits.

nary slope (which would increase with L); this confirms that we are not dealing with a phase transition.

The topological density $q = \langle Q \rangle / V$ is illustrated in Fig. 11 in two ways, as a function of β_{lat} and of $\mu_{B,\text{lat}}$. At $\mu_{B,\text{lat}} = 0$, parity symmetry implies $q = 0$. Obviously, $\mu_{B,\text{lat}} > 0$ enhances q , while increasing β suppresses topological windings, and for $L \geq 12$ it is hardly affected by finite-size effects.

We add that we did not observe any maxima in the topological susceptibility χ_t in the interval of β_{lat} that we explored. So in the massive case, χ_t is not helpful in view of the phase diagram, hence we do not include its plot.

Regarding the phase diagram, we rely on the second derivatives of F which we already considered in the chiral case: the specific heat c_V and the magnetic susceptibility χ_m , given in Eqs. (12) and (13). Figure 12 shows c_V at $\mu_{B,\text{lat}} = 2$: there are no clear peaks, unlike Fig. 5, but we can identify the maxima by Gaussian fits (their uncertainty is estimated by the jackknife method).

Figure 13 is devoted to the thermodynamic extrapolations of these maxima at $\mu_{B,\text{lat}} = 1$ and 2, which lead to

$$\begin{aligned} \beta_{\text{pc,lat}}(\mu_{B,\text{lat}} = 1) &= 0.957(6), \\ \beta_{\text{pc,lat}}(\mu_{B,\text{lat}} = 2) &= 0.951(5). \end{aligned} \quad (20)$$

Similarly, Fig. 14 shows χ_m at $\mu_{B,\text{lat}} = 2$. Again there are no sharp peaks, but here the Gaussian fits work well and provide another criterion for the pseudo-critical values $\beta_{\text{pc,lat}}$. We see that these values are well below the ones obtained from c_V in Fig. 12.

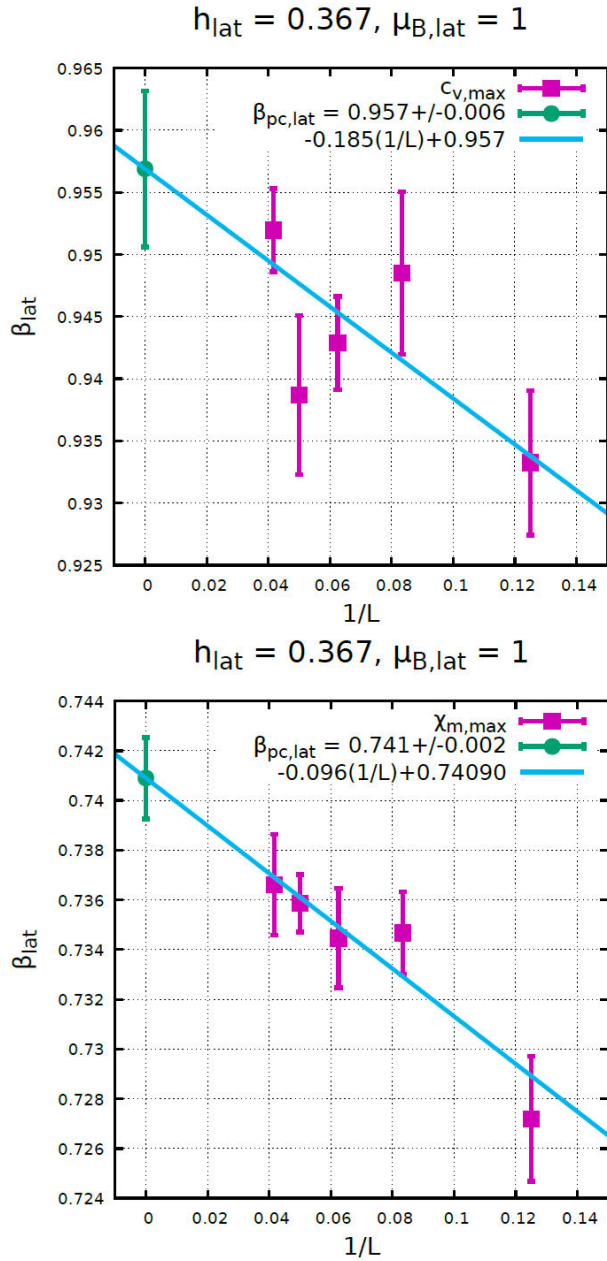


FIGURE 13. Extrapolations of the maxima $\beta_{\text{max,lat}}$ of c_V at $L = 8 \dots 24$ to the large- L limit. This is carried out for each value of $\mu_{B,\text{lat}}$; here we show $\mu_{B,\text{lat}} = 1$ and 2 as examples.

Figure 15 illustrates the large- L extrapolations of these maxima. In these examples, we obtain

$$\begin{aligned} \beta_{\text{pc,lat}}(\mu_{B,\text{lat}} = 1) &= 0.741(2), \\ \beta_{\text{pc,lat}}(\mu_{B,\text{lat}} = 2) &= 0.791(1). \end{aligned} \quad (21)$$

In Figs. 13 and 15 we see slopes which are significantly driven by the result at $L = 8$ — an effect, which we would

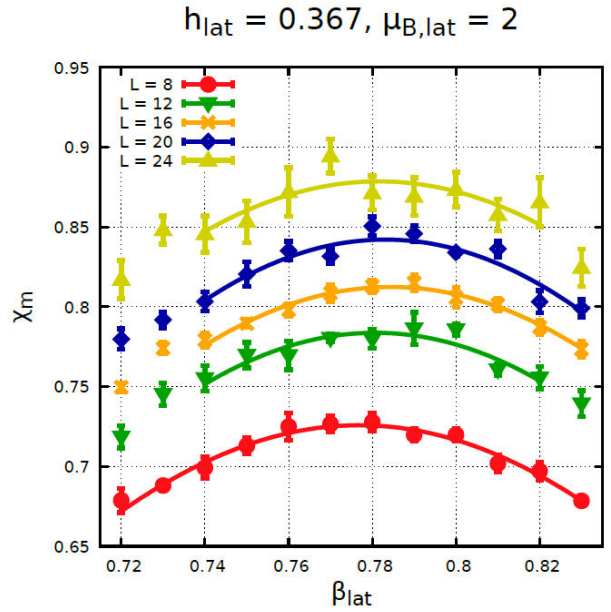


FIGURE 14. The magnetic susceptibility χ_m at $\mu_{B,\text{lat}} = 2$ as a function of β_{lat} , in various volumes. Again we identify the maxima $\beta_{\text{max,lat}}$ by Gaussian fits.

like to overcome. We should soon have results at $L > 24$, which will enable sensible fits excluding $L = 8$. This will improve the validity of the $\beta_{\text{pc,lat}}$ values, although they will change most likely just at percent-level.

As another working hypothesis, we interpret the large- L extrapolated results for $\beta_{\text{pc,lat}}$ based on c_V and on χ_m as boundaries of the crossover interval. We convert $\mu_{B,\text{lat}}$ and $T_{\text{lat}} = 1/\beta_{\text{lat}}$ to physical units, as described in the beginning of this section, and include the corresponding results that we obtained at $h_{\text{lat}} = 0.14$, including $\mu_{B,\text{lat}} = 2.5$. This leads to our conjectured phase diagram in the massive case, which we display in Fig. 16. We recall that $h_{\text{lat}} = 0.14$ and 0.367 (roughly) correspond to the physical quark masses m_u and m_d .

In contrast to the chiral phase diagram in Fig. 8, we see only a weak trend of the crossover interval to bend down to lower temperatures as μ_B increases up to ≈ 300 MeV. On the other hand, just as in the chiral limit, we did not encounter the notorious CEP in the range that we explored so far.

5. Summary and conclusions

We presented a study of the $O(4)$ non-linear σ -model. We have good reasons to assume this model to be in the same universality class as 2-flavor QCD in the chiral limit, because the spontaneous symmetry breaking patterns coincide.ⁱⁱⁱ

ⁱⁱⁱ Due to the dimensions of the Lie groups, $O(N)$ models cannot cope with $N_f > 2$ flavors [16], cf. footnote 1. It is a drawback of this effective theory that we cannot include the s -quark or even heavier quark flavors.

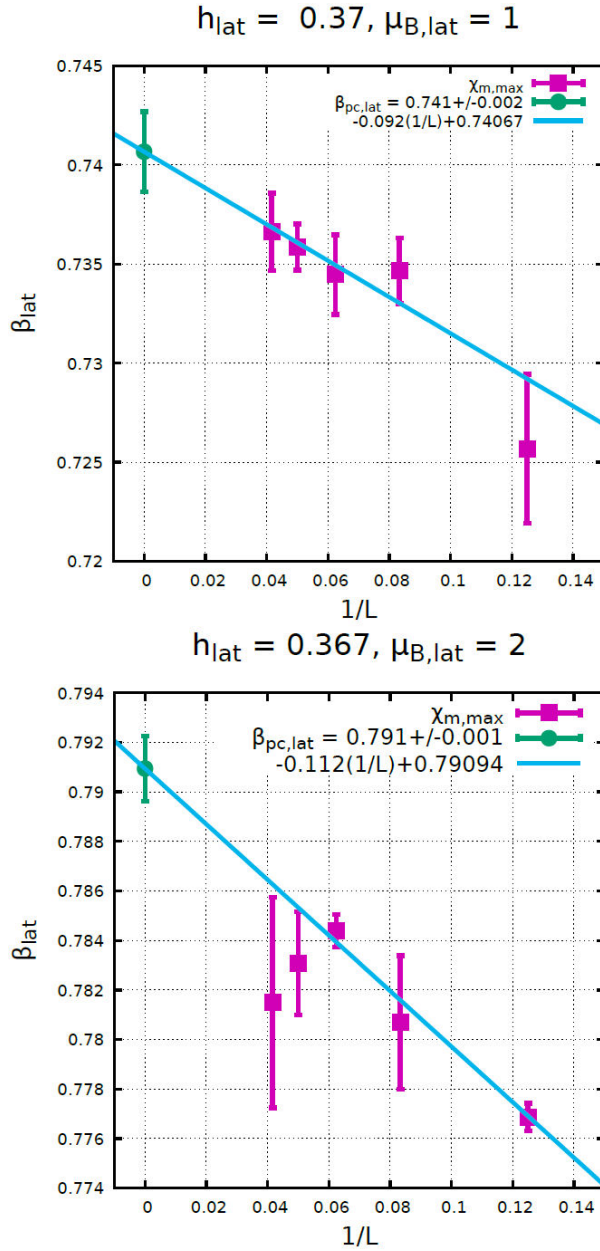


FIGURE 15. Extrapolations of the maxima $\beta_{\text{max,lat}}$ of χ_m at $L = 8 \dots 24$ to the large- L limit. We show the examples at $\mu_{B,\text{lat}} = 1$ and 2.

We are interested in high temperatures, which we assume to be high enough to justify dimensional reduction as a reasonable approximation. This leads to the 3d O(4) model, which has topological charges. They correspond to the baryon number, as Skyrme already knew even before QCD was established [17].^{iv}

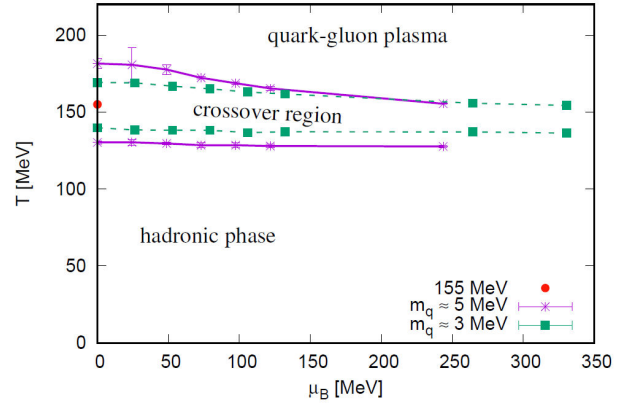


FIGURE 16. Conjectured phase diagram of 2-flavor QCD with degenerate quark masses corresponding to m_u or to m_d .

In this sense, the model can be simulated with a baryon chemical potential $\mu_{B,\text{lat}}$, which corresponds to an imaginary vacuum angle, without any sign problem. As a further advantage, we can apply a powerful cluster algorithm. In the chiral limit, we followed the critical line up to $\mu_B \simeq 309$ MeV, $T_c \simeq 106$ MeV. (We converted lattice units to physical units by referring to the critical temperature at $\mu_B = 0$.)

The result is shown in Fig. 8. The line for $T_c(\mu_B)$ decreases monotonically, in agreement with other conjectures in the literature; this is the generally expected behavior. As far as we could follow this line, we did not find a Critical Endpoint (CEP), but there are hints for it to be near the final point included in our study.

We also investigated the massive case, with degenerate quark masses m_q , which approximately correspond either to m_u or to m_d (this identification involves the chiral condensate, in addition to the pseudo-critical temperature T_{pc}). Here, we identified an interval for the crossover temperature, based on the maxima of two observables, which are given by second derivatives of the free energy F (in the chiral limit, they detect the critical temperature).

We monitored this crossover interval up to $\mu_B \approx 300$ MeV. It is rather broad, see Fig. 16, with only a minor trend towards lower T_{pc} as μ_B increases. Again we could not find a CEP.

An overview over predictions for the CEP temperature and baryonic chemical potential is given in Ref. [30], and compared to the bounds based on our conjecture.

If we manage to extend the numerical study of this effective theory to larger values of μ_B and eventually find a CEP, we could also explore phases at even higher μ_B that the literature speculates about.

^{iv} Skyrme stayed in 4 space-time dimensions, and added a 4-derivative term in order to stabilize the structures in the configurations, which include a 3d spatial instanton.

Acknowledgments

We are indebted to Arturo Fernández Téllez and Miguel Ángel Nava Blanco for their contributions to this project at an early stage. We thank Uwe-Jens Wiese for instructive discussions, and Philippe de Forcrand and Christian Hoelbling for interesting comments. This work was presented by ELC and JAGH at the XXXV *Reunión Anual de la Di-*

visión de Partículas y Campos of the *Sociedad Mexicana de Física*. The simulations were performed on the cluster of the Instituto de Ciencias Nucleares; we thank Luciano Díaz González for technical assistance. We acknowledge support by UNAM-DGAPA through PAPIIT project IG100219, “Exploración teórica y experimental del diagrama de fase de la cromodinámica cuántica”, and by the Consejo Nacional de Ciencia y Tecnología (CONACYT).

1. H.-T. Ding *et al.* (HotQCD Collaboration), Chiral phase transition temperature in (2+1)-Flavor QCD, *Phys. Rev. Lett.* **123** (2019) 062002 <https://doi.org/10.1103/PhysRevLett.123.062002>.
2. A.Yu. Kotov, M.P. Lombardo and A. Trunin, QCD transition at the physical point, and its scaling window from twisted mass Wilson fermions, arXiv:2105.09842 [hep-lat].
3. S. Borsanyi, Z. Fodor, C. Hoelbling, S. D. Katz, S. Krieg, C. Ratti, K. K. Szabo, Is there still any T_c mystery in lattice QCD? Results with physical masses in the continuum limit III, *JHEP* **1009** (2010) 073 [https://doi.org/10.1007/JHEP09\(2010\)073](https://doi.org/10.1007/JHEP09(2010)073). T. Bhattacharya *et al.* (HotQCD Collaboration), QCD Phase Transition with Chiral Quarks and Physical Quark Masses, *Phys. Rev. Lett.* **113** (2014) 082001 <https://doi.org/10.1103/PhysRevLett.113.082001>. A. Bazavov *et al.* (HotQCD Collaboration), Chiral crossover in QCD at zero and non-zero chemical potentials, *Phys. Lett. B* **795** (2019) 15 <https://doi.org/10.1016/j.physletb.2019.05.013>.
4. D. Blaschke *et al.*, Searching for a QCD mixed phase at the Nuclotron-based Ion Collider fAcility (NICA White Paper) 2014 http://mpd.jinr.ru/wp-content/uploads/2016/04/WhitePaper_10.01.pdf. V. Abgaryan *et al.* (MPD Collaboration), Status and initial physics performance studies of the MPD-NICA experiment, in preparation.
5. P. de Forcrand, Simulating QCD at finite density, *PoS LAT2009* (2009) 010 <https://doi.org/10.22323/1.091.0010>. L. Levkova, QCD at nonzero temperature and density, *PoS LATTICE2011* (2011) 011 <https://doi.org/10.22323/1.139.0011>. C. Ratti, Lattice QCD and heavy ion collisions: a review of recent progress, *Rept. Prog. Phys.* **81** (2018) 084301 <https://doi.org/10.1088/1361-6633/aabb97>.
6. C. Laflamme *et al.*, $\mathbb{C}P(N-1)$ quantum field theories with alkaline-earth atoms in optical lattices, *Annals Phys.* **370** (2016) 117 <https://doi.org/10.1016/j.aop.2016.03.012>; Proposal for the Quantum Simulation of the $\mathbb{C}P(2)$ Model on Optical Lattices, *PoS LATTICE2015* (2016) 311 <https://doi.org/10.22323/1.251.0311>.
7. Z.F. Cui, J.L. Zhang and H.S. Zong, Proper time regularization and the QCD chiral phase transition, *Sci. Rep.* **7** (2017) 45937 <https://doi.org/10.1038/srep45937>. J. Braun, M. Leonhardt and M. Pospiech, Fierz-complete NJL model study III: Emergence from quark-gluon dynamics, *Phys. Rev. D* **101** (2020) 036004 <https://doi.org/10.1103/PhysRevD.101.036004>.
8. G.A. Contrera, A.G. Grunfeld and D. Blaschke, Supporting the search for the CEP location with nonlocal PNJL models constrained by lattice QCD, *Eur. Phys. J. A* **52** (2016) 231 <https://doi.org/10.1140/epja/i2016-16231-x>. K. Xu, Z. Li and M. Huang, QCD critical end point from a realistic PNJL model, *EPJ Web Conf.* **192** (2018) 00019 <https://doi.org/10.1051/epjconf/201819200019>. M. Motta, W.M. Alberico, A. Beraudo, P. Costa and R. Stiele, Exploration of the phase diagram and the thermodynamic properties of QCD at finite temperature and chemical potential with the PNJL effective model, *J. Phys. Conf. Ser.* **1667** (2020) 012029 <https://doi.org/10.1088/1742-6596/1667/1/012029>. Y.P. Zhao, S.Y. Zuo and C.M. Li, QCD chiral phase transition and critical exponents within the nonextensive Polyakov-Nambu-Jona-Lasinio model, *Chin. Phys. C* **45** (2021) 073105 <https://doi.org/10.1088/1674-1137/abf8a2>. A. Sarkar, P. Deb and R. Bose, Study of finite volume number density fluctuation at RHIC energies in PNJL model for the search of QCD Critical Point, arXiv:2202.00034 [hep-ph].
9. A. Ayala, S. Hernández-Ortiz and L.A. Hernández, QCD phase diagram from chiral symmetry restoration: analytic approach at high and low temperature using the linear sigma model with quarks, *Rev. Mex. Fis.* **64** (2018) 302 <https://doi.org/10.31349/RevMexFis.64.302>. A. Ayala, S. Hernández-Ortiz, L.A. Hernández, V. Knapp-Pérez and R. Zamora, Fluctuating temperature and baryon chemical potential in heavy-ion collisions and the position of the critical end point in the effective QCD phase diagram, *Phys. Rev. D* **101** (2020) 074023 <https://doi.org/10.1103/PhysRevD.101.074023>. A. Ayala, B. Almeida Zamora, J.J. Cobos-Martínez, S. Hernández-Ortiz, L.A. Hernández, A. Raya and M.E. Tejeda-Yeomans, Collision energy dependence of the critical end point from baryon number fluctuations in the Linear Sigma Model with quarks, *Eur. Phys. J. A* **58** (2022) 87 <https://doi.org/10.1140/epja/s10050-022-00732-8>.
10. O. DeWolfe, S.S. Gubser and C. Rosen, Dynamic critical phenomena at a holographic critical point, *Phys. Rev. D* **84** (2011) 126014 <https://doi.org/10.1103/PhysRevD.84.126014>. R. Critelli, J. Noronha, J. Noronha-Hostler, I. Portillo, C. Ratti and R. Rougemont, Critical point in the phase diagram of primordial quark-gluon matter from black hole physics, *Phys. Rev. D* **96** (2017) 096026 <https://doi.org/10.1103/PhysRevD.96.096026>. Z. Li, K. Xu and M. Huang, The entanglement properties of holographic QCD model with a critical end point, *Chin. Phys. C* **45** (2021) 013116 <https://doi.org/10.1088/1674-1137/abf8a2>.

- //doi.org/10.1088/1674-1137/abc539.
11. P. Kovács and G. Wolf, Phase diagram and isentropic curves from the vector meson extended Polyakov quark meson model, *Acta Phys. Polon. Supp.* **10** (2017) 1107 <https://doi.org/10.5506/APhysPolBSupp.10.1107>.
 12. C. Shi, Y.-L. Du, S.-S. Xu, X.-J. Liu and H.-S. Zong, Continuum study of the QCD phase diagram through an OPE-modified gluon propagator, *Phys. Rev. D* **93** (2016) 036006 <https://doi.org/10.1103/PhysRevD.93.036006>. B.L. Li, Z.F. Cui, B.W. Zhou, S. An, L.P. Zhang and H.S. Zong, Finite volume effects on the chiral phase transition from Dyson-Schwinger equations of QCD, *Nucl. Phys. B* **938** (2019) 298 <https://doi.org/10.1016/j.nuclphysb.2018.11.015>. Y.P. Zhao, R.R. Zhang, H. Zhang and H.S. Zong, Chiral phase transition from the Dyson-Schwinger equations in a finite spherical volume, *Chin. Phys. C* **43** (2019) 063101 <https://doi.org/10.1088/1674-1137/43/6/063101>. C. Shi, X.-T. He, W.-B. Jia, Q.-W. Wang, S.-S. Xu and H.-S. Zong, Chiral transition and the chiral charge density of the hot and dense QCD matter, *JHEP* **06** (2020) 122 [https://doi.org/10.1007/JHEP06\(2020\)122](https://doi.org/10.1007/JHEP06(2020)122). F. Gao and J.M. Pawłowski, QCD phase structure from functional methods *Phys. Rev. D* **102** (2020) 034027 <https://doi.org/10.1103/PhysRevD.102.034027>.
 13. Z.Q. Wu, J.L. Ping and H.S. Zong, QCD phase diagram at finite isospin and baryon chemical potentials with the self-consistent mean field approximation. *Chin. Phys. C* **45** (2021) 064102 <https://doi.org/10.1088/1674-1137/abefc3>.
 14. E.S. Fraga, L.F. Palhares and P. Sorensen, Finite-size scaling as a tool in the search for the QCD critical point in heavy ion data, *Phys. Rev. C* **84** (2011) 011903 <https://doi.org/10.1103/PhysRevC.84.011903>. N.G. Antoniou, F.K. Diakonou, X.N. Maintas and C.E. Tsagkarakis, Locating the QCD critical endpoint through finite-size scaling, *Phys. Rev. D* **97** (2018) 034015 <https://doi.org/10.1103/PhysRevD.97.034015>.
 15. R. D. Pisarski and F. Wilczek, Remarks on the chiral phase transition in chromodynamics, *Phys. Rev. D* **29** (1984) 338 <https://doi.org/10.1103/PhysRevD.29.338>. F. Wilczek, Application of the renormalization group to a second order QCD phase transition, *Int. J. Mod. Phys. A* **7** (1992) 3911 <https://doi.org/10.1142/S0217751X92001757> [Erratum: *Int. J. Mod. Phys. A* **7** (1992) 6951 <https://doi.org/10.1142/S0217751X92003665>]. K. Rajagopal and F. Wilczek, Static and dynamic critical phenomena at a second order QCD phase transition, *Nucl. Phys. B* **399** (1993) 395 [https://doi.org/10.1016/0550-3213\(93\)90502-G](https://doi.org/10.1016/0550-3213(93)90502-G). A. Yu. Kotov, M. P. Lombardo and A. Trunin, Gliding Down the QCD Transition Line, from $N_f = 2$ till the Onset of Conformality, *Symmetry* **13** (2021) 1833 <https://doi.org/10.3390/sym13101833>.
 16. W. Bietenholz, On the Isomorphic Description of Chiral Symmetry Breaking by Non-Unitary Lie Groups, *Int. J. Mod. Phys. A* **25** (2010) 1699 <https://doi.org/10.1142/S0217751X10048123>.
 17. T. H. R. Skyrme, A Nonlinear field theory, *Proc. Roy. Soc. Lond. A* **260** (1961) 127 <https://doi.org/10.1098/rspa.1961.0018>; A unified field theory of mesons and baryons, *Nucl. Phys.* **31** (1962) 556 [https://doi.org/10.1016/0029-5582\(62\)90775-7](https://doi.org/10.1016/0029-5582(62)90775-7). G. S. Adkins, C. R. Nappi and E. Witten, Static properties of nucleons in the Skyrme model, *Nucl. Phys. B* **228** (1983) 552 [https://doi.org/10.1016/0550-3213\(83\)90559-X](https://doi.org/10.1016/0550-3213(83)90559-X). I. Zahed and G.E. Brown, The Skyrme Model, *Phys. Rept.* **142** (1986) 1 [https://doi.org/10.1016/0370-1573\(86\)90142-0](https://doi.org/10.1016/0370-1573(86)90142-0).
 18. B. Berg and M. Lüscher, Definition and Statistical Distributions of a Topological Number in the Lattice O(3) Sigma Model, *Nucl. Phys. B* **190** (1981) 412 [https://doi.org/10.1016/0550-3213\(81\)90568-X](https://doi.org/10.1016/0550-3213(81)90568-X).
 19. J. Murakami, Volume formulas for a spherical tetrahedron, *Proc. Amer. Math. Soc.* **140** (2012) 3289 <https://doi.org/10.1090/S0002-9939-2012-11182-7>.
 20. M. A. Nava Blanco, W. Bietenholz and A. Fernández Téllez, Conjecture about the 2-Flavour QCD Phase Diagram, *J. Phys. Conf. Ser.* **912** (2017) 012048 <https://doi.org/10.1088/1742-6596/912/1/012048>. M. A. Nava Blanco, Estudio del diagrama de fase de QCD con dos sabores usando el modelo 3d O(4), M.Sc. thesis, Benemérita Universidad Autónoma de Puebla, 2019.
 21. U. Wolff, Collective Monte Carlo Updating for Spin Systems, *Phys. Rev. Lett.* **62** (1989) 361 <https://doi.org/10.1103/PhysRevLett.62.361>.
 22. C.M. Fortuin and P.W. Kasteleyn, On the random-cluster model: I. Introduction and relation to other models, *Physica* **57** (1972) 536 [https://doi.org/10.1016/0031-8914\(72\)90045-6](https://doi.org/10.1016/0031-8914(72)90045-6).
 23. E. López-Contreras, Phase Diagram of the 3d O(4) model as a conjecture for Quantum Chromodynamics in the chiral limit, B.Sc. thesis, Universidad Nacional Autónoma de México, 2021.
 24. K. Kanaya and S. Kaya, Critical exponents of a three-dimensional O(4) spin model, *Phys. Rev. D* **51** (1995) 2404 <https://doi.org/10.1103/PhysRevD.51.2404>.
 25. M. Oevers, Kritisches Verhalten in O(4)-symmetrischen Spinmodellen und 2-flavour QCD, Diploma thesis, Universität Bielefeld, 1996.
 26. J. Engels, L. Fromme and M. Seniuch, Correlation lengths and scaling functions in the three-dimensional O(4) model, *Nucl. Phys. B* **675** (2003) 533 <https://doi.org/10.1016/j.nuclphysb.2003.09.060>.
 27. K. Binder and D.W. Heermann, Monte Carlo Simulation in Statistical Physics, Springer, 1997.
 28. J.-S. Wang, Clusters in the three-dimensional Ising model with a magnetic field, *Physica A* **161** (1989) 249 [https://doi.org/10.1016/0378-4371\(89\)90468-8](https://doi.org/10.1016/0378-4371(89)90468-8).
 29. J.A. García-Hernández, Conjecture about the Quantum Chromodynamics Phase Diagram with two Light Quark Flavors, B.Sc. thesis, Universidad Nacional Autónoma de México, 2020.
 30. J. A. García-Hernández, E. López-Contreras, E. N. Polanco-Euán and W. Bietenholz, Conjecture about the QCD phase diagram, *PoS LAT2021 (2021)* 595. <https://doi.org/10.48550/arXiv.2111.01954>.